

## One-Dimensional Coordination Polymers from Hexanuclear Manganese Carboxylate Clusters Featuring a $\{\text{Mn}^{\text{II}}_4\text{Mn}^{\text{III}}_2(\mu_4\text{-O})_2\}$ Core and Spacer Linkers

Iurii L. Malaestean,<sup>†</sup> Victor Ch. Kravtsov,<sup>‡</sup> Manfred Speldrich,<sup>†</sup> Galina Dulcevscaia,<sup>§</sup> Yurii A. Simonov,<sup>‡</sup> Janusz Lipkowski,<sup>||</sup> Arkady Ellern,<sup>⊥</sup> Svetlana G. Baca,<sup>§</sup> and Paul Kögerler<sup>\*,†</sup>

<sup>†</sup>*Institute of Inorganic Chemistry, RWTH Aachen University, D-52074 Aachen, Germany,*

<sup>‡</sup>*Institute of Applied Physics, and* <sup>§</sup>*Institute of Chemistry, Academy of Sciences of Moldova, MD-2028 Chisinau, Moldova,* <sup>||</sup>*Institute of Physical Chemistry, Polish Academy of Sciences, 01-224 Warsaw, Poland, and*

<sup>⊥</sup>*Department of Chemistry, Iowa State University, Ames, Iowa 50011*

Received March 22, 2010

The bridging of hexanuclear mixed-valent carboxylate coordination clusters of the type  $[\text{Mn}_6\text{O}_2(\text{O}_2\text{CR})_{10}]$  ( $\text{R} = \text{CMe}_3; \text{CHMe}_2$ ) featuring a  $\{\text{Mn}^{\text{II}}_4\text{Mn}^{\text{III}}_2(\mu_4\text{-O})_2\}$  core by geometrically rigid as well as flexible spacer ligands such as pyrazine (pyz), nicotinamide (na), or 1,2-bis(4-pyridyl)ethane (bpe) results exclusively in one-dimensional (1D) coordination polymers. The formation of  $\{[\text{Mn}_6\text{O}_2(\text{O}_2\text{CCMe}_3)_{10}(\text{Me}_3\text{CCO}_2\text{H})(\text{EtOH})(\text{na})] \cdot \text{EtOH} \cdot \text{H}_2\text{O}\}_n$  (**1**),  $\{[\text{Mn}_6\text{O}_2(\text{O}_2\text{CCHMe}_2)_{10}(\text{pyz})_3] \cdot \text{H}_2\text{O}\}_n$  (**2**), and  $\{[\text{Mn}_6\text{O}_2(\text{O}_2\text{CCHMe}_2)_{10}(\text{Me}_2\text{CHCO}_2\text{H})(\text{EtOH})(\text{bpe})] \cdot \text{Me}_2\text{CHCO}_2\text{H}\}_n$  (**3**) illustrates a surprising preference of the interlinked  $\{\text{Mn}_6\}$  units toward 1D coordination chains. In the solid-state, the observed chain propagation axes are either colinear (**1** and **3**) or perpendicular (**2**), whereby crystal packing is further influenced by solvent molecules. Magnetic properties of these network compounds can be rationalized based on that the magnetism of discrete  $[\text{Mn}_6\text{O}_2(\text{O}_2\text{CR})_{10}]$ -type coordination clusters with all-antiferromagnetic intramolecular exchange and weak antiferromagnetic intercluster coupling in **1**, **2**, and **3** follows the expected exchange coupling strength of the employed spacer linkers.

### Introduction

The past decade has witnessed tremendous advances in the development of metal–organic materials (MOMs), also known as coordination polymers, hybrid inorganic–organic materials, and metal–organic frameworks (MOFs). They captured broad attention as it became evident that MOMs are typically facile to prepare and, because of their inherent modularity, prototypical for a diverse range of structures that are amenable to crystal engineering design strategies. MOMs are primarily constructed from mononuclear metal centers and organic ligands, and this has resulted in a tremendous number of intriguing network topologies and a variety of packing

motifs<sup>1</sup> along with potential applications as functional materials.<sup>2</sup> In particular, porous MOF solids emerged as an independent research area.<sup>3</sup> Recently, more attention has been paid to expand the classical Aufbau principles to include polynuclear coordination clusters as building units, with the

\*To whom correspondence should be addressed. E-mail: paul.koegerler@ac.rwth-aachen.de.

(1) (a) Hoskins, B. F.; Robson, R. *J. Am. Chem. Soc.* **1990**, *112*, 1546. (b) Yaghi, O. M.; Li, H.; Davis, C.; Richardson, D.; Groy, T. L. *Acc. Chem. Res.* **1998**, *31*, 474. (c) Moulton, B.; Zaworotko, M. J. *Chem. Rev.* **2001**, *101*, 1629. (d) Batten, S. R. *CrystEngComm* **2001**, *3*, 67. (e) Carlucci, L.; Ciani, G.; Proserpio, D. M. *Coord. Chem. Rev.* **2003**, *246*, 247. (f) Batten, S. R.; Robson, R. *Angew. Chem., Int. Ed.* **1998**, *37*, 1460. (g) Batten, S. R.; Jeffery, J. C.; Ward, M. D. *Inorg. Chim. Acta* **1999**, *292*, 231. (h) O'Keeffe, M.; Eddaoudi, M.; Li, H. L.; Reinecke, T.; Yaghi, O. M. *J. Solid State Chem.* **2000**, *152*, 3. (i) Zaworotko, M. J. *Chem. Commun.* **2001**, 1. (j) Cheetham, A. K.; Rao, C. N. R.; Feller, R. K. *Chem. Commun.* **2006**, 4780. (k) Surlbe, S.; Serre, C.; Mellot-Draznié, C.; Millange, F.; Férey, G. *Chem. Commun.* **2006**, 284. (l) Maji, T. K.; Matsuda, R.; Kitagawa, S. *Nat. Mater.* **2007**, *6*, 142. (m) Yaghi, O. M. *Nat. Mater.* **2007**, *6*, 92. (n) Rao, K. P.; Thirumurugan, A.; Rao, C. N. R. *Chem.—Eur. J.* **2007**, *13*, 3193. (o) Luisi, B. L.; Kravtsov, V. Ch.; Moulton, B. D. *Cryst. Growth Des.* **2006**, *6*, 2207.

(2) (a) Kitagawa, S.; Kitaura, R.; Noro, S. *Angew. Chem., Int. Ed.* **2004**, *43*, 2334. (b) Evans, O. R.; Lin, W. *Acc. Chem. Res.* **2002**, *35*, 511. (c) Janiak, C. *Dalton Trans.* **2003**, 2781. (d) Chen, C. T.; Suslick, K. S. *Coord. Chem. Rev.* **1993**, *128*, 293. (e) Seo, J. S.; Whang, D.; Lee, H.; Jun, S. I.; Oh, J.; Jeon, Y. J.; Kim, K. *Nature* **2000**, *404*, 982. (f) Kahn, O.; Martínez, C. *Science* **1998**, *279*, 44. (g) Fallah, M. S. E.; Rentschler, E.; Caneschi, A.; Sessoli, R.; Gatteschi, D. *Angew. Chem., Int. Ed. Engl.* **1996**, *35*, 1947. (h) Fujita, M.; Kwon, Y. J.; Washizu, S.; Ogura, K. *J. Am. Chem. Soc.* **1994**, *116*, 1151. (i) Noro, S.; Kitagawa, S.; Kondo, M.; Seki, K. *Angew. Chem., Int. Ed.* **2000**, *39*, 2081. (j) Kondo, M.; Shimamura, M.; Noro, S.; Minakoshi, S.; Asami, A.; Seki, K.; Kitagawa, S. *Chem. Mater.* **2000**, *12*, 1288. (k) Forster, P. M.; Eckert, J.; Heiken, B. D.; Parise, J. B.; Yoon, J. W.; Jung, S. H.; Chang, J.-S.; Cheetham, A. K. *J. Am. Chem. Soc.* **2006**, *128*, 16846. (l) Cheetham, A. K.; Rao, C. N. R. *Science* **2007**, *318*, 58. (m) Férey, G.; Millange, F.; Morcrette, M.; Serre, C.; Doublet, M.-L.; Greneche, J.-M.; Tarascon, J.-M. *Angew. Chem., Int. Ed.* **2007**, *46*, 3259. (n) Horcajada, P.; Serre, C.; Vallet-Regi, M.; Sebban, M.; Tauler, F.; Férey, G. *Angew. Chem., Int. Ed.* **2006**, *45*, 5974. (o) Tanaka, D.; Kitagawa, S. *MRS Bull.* **2007**, *32*, 4670. (p) Hayashi, H.; Cote, A. P.; Furukawa, H.; O'Keeffe, M.; Yaghi, O. M. *Nat. Mater.* **2007**, *6*, 501. (q) Chen, B.; Liang, C.; Yang, J.; Contreras, D. S.; Clancy, Y. L.; Lobkovsky, E. B.; Yaghi, O. M.; Dai, S. *Angew. Chem., Int. Ed.* **2006**, *45*, 1390. (r) Rowsell, J. L. C.; Yaghi, O. M. *Angew. Chem., Int. Ed.* **2005**, *44*, 4670. (s) Mark Thomas, K. *Dalton Trans.* **2009**, 1487. (t) Teichert, O.; Sheldrick, W. S. *Z. Anorg. Allg. Chem.* **2000**, *626*, 1509.

(3) (a) Férey, G. *Chem. Soc. Rev.* **2008**, *37*, 191. (b) Rao, C. N. R.; Natarajan, S.; Vaidhyanathan, R. *Angew. Chem., Int. Ed.* **2004**, *43*, 1466.

intent to utilize them as nodes in the design of polymeric materials. This represents an extension of Robson's classical *node and spacer* approach<sup>4</sup> giving rise to a family of cluster based polymers with enhanced variety of coordination algorithms compared with single metal ions, and the node's size starting from binuclear complexes<sup>5</sup> up to 24-membered nanosphere clusters.<sup>6</sup> In accordance with Ferey's approach, known as "scale chemistry" concept,<sup>7</sup> one can in general anticipate that the same topology of coordination polymer structure may result in larger pores if larger nodes are used. In addition, polynuclear clusters can add their inherent physical characteristics

such as versatile redox properties to the polymeric network,<sup>8</sup> which expands the range of potential practical applications,<sup>9</sup> for example, as low-density magnetic nanoporous materials and magnetic sensors.<sup>10</sup>

Our study focuses on the networking of a class of particularly stable {Mn<sub>6</sub>} coordination clusters that feature a thermodynamically stable {Mn<sup>II</sup><sub>4</sub>Mn<sup>III</sup><sub>2</sub>(μ<sub>4</sub>-O)<sub>2</sub>} core.<sup>11</sup> This allows us to employ a range of bridging ligands without risking decomposition or rearrangement of the {Mn<sub>6</sub>} cage-like motif. Hexanuclear manganese carboxylate [Mn<sub>6</sub>O<sub>2</sub>(O<sub>2</sub>CR)<sub>10</sub>L<sub>4</sub>] clusters (L: neutral monodentate ligand) represent attractive candidates for the construction of cluster-based polymeric materials because of several characteristics: (i) interesting magnetic properties, (ii) modification with respect to size and solution properties by judicious choice of RCO<sub>2</sub><sup>-</sup> carboxylate and capping ligands, while the topology of the cluster skeleton remains invariant, (iii) the four capping ligands L in such clusters may be completely or partially replaced, thus [Mn<sub>6</sub>O<sub>2</sub>(O<sub>2</sub>CR)<sub>10</sub>] fragments might be viewed as tectonic building blocks with connectivity up to four. Use of appropriate exobidentate spacer ligands instead of monodentate capping ligands allows interlinking clusters to dumbbell-like dimers, polymeric chains, and 3D diamond-like frameworks.<sup>12,13</sup> Among the latter, heterospin compounds with nitronyl nitroxide radical molecules as exobidentate spacer ligands<sup>12</sup> display single-molecular magnet properties. Moreover, it has been shown that because of partial decomposition of [Mn<sub>6</sub>O<sub>2</sub>(O<sub>2</sub>CR)<sub>10</sub>L<sub>4</sub>] clusters under solvothermal conditions one propionate ligand can change its function from intracuster to intercluster bridging, resulting in a one-dimensional (1D) chain polymer with a Mn···Mn 4.88 Å intercluster intrachain separation.<sup>14</sup>

Recently we reported a series of chain coordination polymers build up from tri- and tetranuclear manganese carboxylate cluster blocks with {Mn<sub>3</sub>}, {Mn<sub>3</sub>O}, and {Mn<sub>4</sub>O<sub>2</sub>} cores bridged by 2,2'-bipyrimidine or hexamethylenetetramine ligands<sup>15a</sup> as well as polynuclear coordination clusters.<sup>15b,c</sup> In continuing our research on the design of coordination polymers from carboxylate clusters, we report the synthesis, structure and magnetic properties of three novel 1D chain coordination polymers based on hexanuclear manganese carboxylate clusters with a common {Mn<sup>II</sup><sub>4</sub>Mn<sup>III</sup><sub>2</sub>(μ<sub>4</sub>-O)<sub>2</sub>} core and the N-heteroaromatic *exo*-bidentate spacer ligands nicotinamide (na), pyrazine (pyz), and 1,2-bis(4-pyridyl)ethane (bpe) as spacer ligands. The resulting 1D networks (symbol <sup>10</sup>O<sup>f</sup> according to ref 1j) are isolated as {[Mn<sub>6</sub>O<sub>2</sub>(O<sub>2</sub>CCMe<sub>3</sub>)<sub>10</sub>(Me<sub>3</sub>CCO<sub>2</sub>H)(EtOH)(na)]·EtOH·H<sub>2</sub>O}<sub>n</sub> (**1**), {[Mn<sub>6</sub>O<sub>2</sub>(O<sub>2</sub>CCHMe<sub>2</sub>)<sub>10</sub>(pyz)<sub>3</sub>]·2H<sub>2</sub>O}<sub>n</sub> (**2**), and {[Mn<sub>6</sub>O<sub>2</sub>(O<sub>2</sub>CCHMe<sub>2</sub>)<sub>10</sub>(Me<sub>2</sub>CHCO<sub>2</sub>H)(EtOH)(bpe)]·Me<sub>2</sub>CHCO<sub>2</sub>H}<sub>n</sub> (**3**).

(4) (a) Gable, R. W.; Hoskins, B. F.; Robson, R. *J. Chem. Soc., Chem. Commun.* **1990**, 1677. (b) Robson, R. *J. Chem. Soc., Dalton Trans.* **2000**, 3735.

(5) (a) Tudor, V.; Marin, G.; Kravtsov, V.; Simonov, Yu. A.; Lipkowski, J.; Brezeanu, M.; Andruh, M. *Inorg. Chim. Acta* **2003**, 353, 35. (b) Marin, G.; Tudor, V.; Kravtsov, V. Ch.; Schmidtman, M.; Simonov, Yu. A.; Müller, A.; Andruh, M. *Cryst. Growth Des.* **2005**, 5, 279.

(6) (a) McManus, G. J.; Wang, Z.; Zaworotko, M. J. *Cryst. Growth Des.* **2004**, 4, 11. (b) Perry, J. J.; Kravtsov, V. Ch.; McManus, G. J.; Zaworotko, M. J. *J. Am. Chem. Soc.* **2007**, 129, 10076.

(7) Ferey, G. *J. Solid State Chem.* **2000**, 152, 37.

(8) (a) Wang, S.; Tsai, H.-L.; Foltling, K.; Martin, J. D.; Hendrickson, D. N.; Christou, G. *J. Chem. Soc., Chem. Commun.* **1994**, 671. (b) L., F.; Prescimone, A.; Evangelisti, M.; Brechin, E. K. *Chem. Commun.* **2009**, 2023. (c) Zhang, J. J.; Lachgar, A. *J. Am. Chem. Soc.* **2007**, 129, 250. (d) Zhang, X. M.; Fang, R. Q.; Wu, H. S. *J. Am. Chem. Soc.* **2005**, 127, 7670. (e) Beauvais, L. G.; Shores, M. P.; Long, J. R. *J. Am. Chem. Soc.* **2000**, 122, 2763. (f) Tao, J.; Tong, M.-L.; Shi, J.-X.; Chen, X.-M. *Chem. Commun.* **2000**, 2043. (g) Tao, J.; Shi, J.-X.; Tong, M.-L.; Zhang, X.-X.; Chen, X.-M. *Inorg. Chem.* **2001**, 40, 6328. (h) Schmitt, W.; Baisa, E.; Mandel, A.; Anson, C. E.; Powell, A. K. *Angew. Chem., Int. Ed.* **2001**, 40, 3578. (i) Carlucci, L.; Ciani, G.; Proserpio, D. M.; Rizzato, S. *Chem. Commun.* **2000**, 1319. (j) Niu, Y. Y.; Song, Y. L.; How, H. W.; Zhu, Y. *Inorg. Chem.* **2005**, 44, 2553. (k) Barthelet, K.; Marrot, J.; Riou, D.; Férey, G. *Angew. Chem., Int. Ed.* **2002**, 41, 281. (l) Dai, J. C.; Wu, X. T.; Cui, C. P.; Hu, S. M.; Du, W. X.; Wu, L. M.; Zhang, H. H.; Sun, R. Q. *Inorg. Chem.* **2002**, 41, 1391. (m) Tong, M.-L.; Shi, J.-X.; Chen, X.-M. *New J. Chem.* **2002**, 26, 814. (n) Livage, C.; Guillou, N.; Chaigneau, J.; Rabu, P. *Mater. Res. Bull.* **2006**, 41, 981. (m) Ma, C.-B.; Chen, C.-N.; Liu, Q.-T.; Liao, D.-Z.; Li, L.-C. *Eur. J. Inorg. Chem.* **2008**, 1865.

(9) (a) Park, K. S.; Ni, Z.; Côté, A. P.; Choi, J. Y.; Huang, R.; Uribe-Romo, F. J.; Chae, H. K.; O'Keefe, M.; Yaghi, O. M. *PNAS* **2006**, 103, 20173. (b) Li, H.; Eddaoudi, M.; O'Keefe, M.; Yaghi, O. M. *Nature* **1999**, 402, 276. (c) Tao, J.; Yin, X.; Wei, Z. B.; Huang, R. B.; Zheng, L. S. *Eur. J. Inorg. Chem.* **2004**, 125.

(10) Maspoch, D.; Ruiz-Molina, D.; Veciana, J. *J. Mater. Chem.* **2004**, 14, 2713.

(11) (a) Baikie, A. R. E.; Howes, A. J.; Hursthouse, M. B.; Quick, A. B.; Thornton, P. *Chem. Commun.* **1986**, 21, 1587. (b) Schake, A. R.; Vincent, J. B.; Li, Q.; Boyd, P. D. W.; Foltling, K.; Huffman, J. C.; Hendrickson, D. N.; Christou, G. *Inorg. Chem.* **1989**, 28, 1915. (c) Batsanov, A. S.; Struchkov, Yu. T.; Timco, G. A.; Gerbeleu, N. V.; Manole, O. S.; Grebenko, S. V. *Koord. Khim. (Russ.)* **1994**, 20, 604. (d) Poyraz, M.; Sari, M.; Cevik, S.; Buyukgungor, O. *Acta Crystallogr.* **2006**, E62, m1442. (e) Murrie, M.; Parsons, S.; Winpenny, R. E. P. *J. Chem. Soc., Dalton Trans.* **1998**, 1423. (f) Kohler, K.; Roesky, H. W.; Noltemeyer, M.; Schmidt, H.-G.; Freire-Erdbrugger, C.; Sheldrick, G. M. *Chem. Ber.* **1993**, 126, 921. (g) Gavrilenko, K. S.; Punin, S. V.; Cadon, O.; Golhen, S.; Ouahab, L.; Pavilshchuk, V. V. *Inorg. Chem.* **2005**, 44, 5903. (h) Gerbier, P.; Ruiz-Molina, D.; Gomez, J.; Wurst, K.; Veciana, J. *Polyhedron* **2003**, 22, 1951. (i) Kiskin, M. A.; Sidorov, A. A.; Fomina, I. G.; Rusinov, G. L.; Ishmetova, R. I.; Aleksandrov, G. G.; Shvedenkov, Yu. G.; Dobrokhotova, Zh. V.; Novotortsev, V. M.; Chupakhin, O. N.; Eremenko, I. L.; Moiseev, I. I. *Inorg. Chem. Commun.* **2005**, 8, 524. (j) Stamatatos, T. C.; Foguet-Albiol, D.; Perlepes, S. P.; Raptopoulou, C. P.; Terzis, A.; Patrickios, C. S.; Christou, G.; Tasiopoulos, A. J. *Polyhedron* **2006**, 25, 1737. (k) Kiskin, M. A.; Fomina, I. G.; Aleksandrov, G. G.; Sidorov, A. A.; Novotortsev, V. M.; Rakiitin, Y. V.; Dobrokhotova, Z. V.; Ikorskii, V. N.; Shvedenkov, Y. G.; Eremenko, I. L.; Moiseev, I. I. *Inorg. Chem. Commun.* **2005**, 8, 89. (l) Kim, J.; Cho, H. *Inorg. Chem. Commun.* **2004**, 7, 122. (m) Nakata, K.; Miyasaka, H.; Ishii, T.; Yamashita, M.; Awaga, K. *Mol. Cryst. Liq. Cryst. Sci. Technol., Sect. A* **2002**, 379, 211. (n) Karsten, P.; Strahle, F. *Acta Crystallogr.* **1998**, C54, 1403. (o) Nakata, K.; Miyasaka, H.; Iwahori, F.; Sugiura, K.; Yamashita, M. *Polyhedron* **2005**, 24, 2250. (p) Fursova, E.; Ovcharenko, V.; Nosova, K.; Romanenko, G.; Ikorskii, V. *Polyhedron* **2005**, 24, 2084. (q) Halcrow, M. A.; Streib, W. E.; Foltling, K.; Christou, G. *Acta Crystallogr.* **1995**, C51, 1263.

(12) Ovcharenko, V.; Fursova, E.; Romanenko, G.; Ikorskii, V. *Inorg. Chem.* **2004**, 43, 3332.

(13) Nakata, K.; Miyasaka, H.; Sugimoto, K.; Ishii, T.; Sugiura, K.; Yamashita, M. *Chem. Lett.* **2002**, 658.

(14) Ma, C. B.; Hu, M. Q.; Chen, H.; Chen, C. N.; Liu, Q. T. *Eur. J. Inorg. Chem.* **2008**, 5274.

(15) (a) Baca, S. G.; Malaestean, I. L.; Keene, T. D.; Adams, H.; Ward, M. D.; Hauser, J.; Neels, A.; Decurtins, S. *Inorg. Chem.* **2008**, 47, 11108. (b) Baca, S. G.; Stoekli-Evans, H.; Ambrus, Ch.; Malinovskii, S. T.; Malaestean, I.; Gerbeleu, N.; Decurtins, S. *Polyhedron* **2006**, 25, 3617. (c) Malaestean, I. L.; Speldrich, M.; Ellern, A.; Baca, S. G.; Ward, M.; Kögerler, P. *Eur. J. Inorg. Chem.* **2009**, 4209. (d) Baca, S. G.; Sevryugina, Yu.; Clerac, R.; Malaestean, I.; Gerbeleu, N.; Petrukhina, M. A. *Inorg. Chem. Commun.* **2005**, 8, 474.

(16) (a) Deacon, G. B.; Philips, R. J. *Coord. Chem. Rev.* **1980**, 33, 227. (b) Mehrotra, R. C.; Bohra, R. *Metal Carboxylates*; Academic Press, New York, 1983; p 47. (c) Nakamoto, K. *Infrared and Raman Spectra of Inorganic and Coordination Compounds*; Wiley: New York, 1986; p 236.

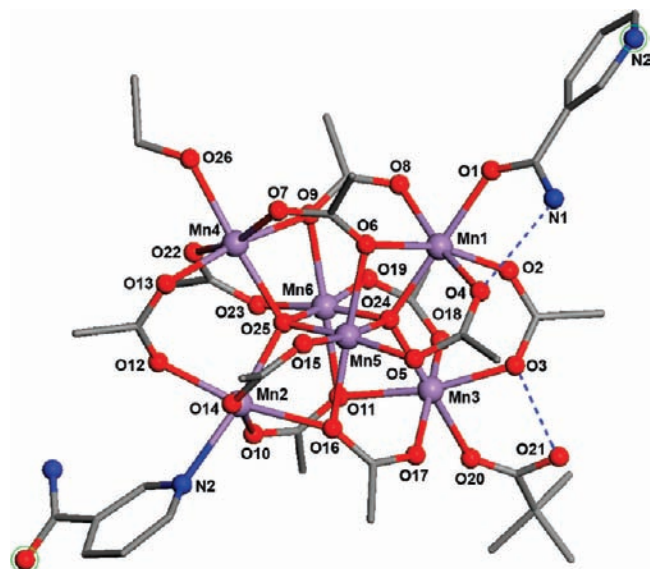


**Figure 1.** Cluster unit in **1** with *trans*-positioned na spacer ligands. *tert*-Butyl groups of bridging pivalate ligands, hydrogen atoms and solvate ethanol and water molecules are omitted for clarity. Only one position of disordered pivalic acid molecule is shown. Green circles indicate bridging ligand donor positions binding to the adjacent {Mn<sub>6</sub>} units in the polymer. Color codes: Mn, violet; O, red; N, blue; C, gray.

## Results and Discussion

**Syntheses and Preliminary Characterization.** All coordination polymers **1–3** are prepared by the reaction of manganese(II) pivalate or isobutyrate salts with appropriate bridging ligands in different solvents. Compound **1** is prepared by interaction of manganese(II) pivalate with nicotina in MeCN/EtOH (1:1) mixture under reflux for 1 h. Using manganese(II) isobutyrate as starting materials, we isolated compounds **2** and **3** by the interaction with pyrazine or 1,2-bis(4-pyridyl)ethane in MeCN or THF/EtOH (1:1) solutions, respectively. The materials were characterized by X-ray diffraction studies, elemental analysis, and IR spectra<sup>16</sup> to confirm the homogeneity of the obtained solids.

**Crystal Structures.** Single-crystal X-ray diffraction analysis reveals that compounds **1–3** comprise 1D chain polymers, which are built up from virtually isostructural [Mn<sub>6</sub>O<sub>2</sub>(O<sub>2</sub>CR)<sub>10</sub>] (R = CMe<sub>3</sub>; CHMe<sub>2</sub>) coordination clusters bearing two capping ligands and linked by exobidentate na, pyz, and bpe spacer ligands, respectively (Figures 1–3). The clusters contain a {Mn<sup>II</sup><sub>4</sub>Mn<sup>III</sup><sub>2</sub>O<sub>2</sub>}<sup>10+</sup> core of two edge-sharing distorted (flattened) Mn<sub>4</sub> tetrahedra, with a μ<sub>4</sub>-O<sup>2-</sup> ion in the center of each tetrahedron. Peripheral ligation is provided by 10 bridging pivalate (**1**) or isobutyrate (**2**, **3**) monoanionic ligands. Four of them are coordinating in η<sup>1</sup>:η<sup>2</sup>:μ<sub>3</sub> mode and bridge three Mn centers whereas the other six each bridge two Mn centers in η<sup>1</sup>:η<sup>1</sup>:μ<sub>2</sub> mode. Within the core, the two central Mn centers are in the oxidation state +III, and the four terminal Mn atoms are in the lower oxidation state +II. Manganese oxidation states are consistent with charge balance and bond parameters (four Mn<sup>III</sup>–O distances are essentially shorter than Mn<sup>II</sup>–O distances, Supporting Information, Table S2), and were confirmed by bond valence sum (BVS) calculations using two different sets of empirical bond-valence parameters, see refs 17 and 18, and

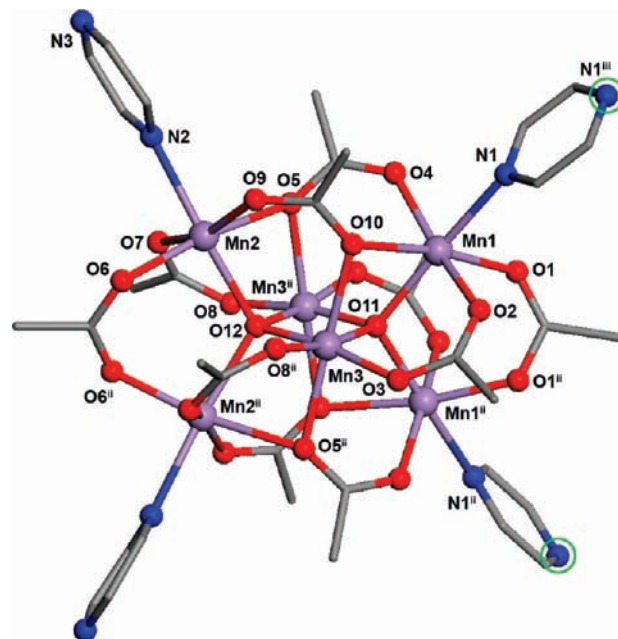


**Figure 2.** Cluster unit in **2** with exobidentate pyz spacers attached to Mn1 and Mn1<sup>II</sup>, and terminal monodentate pyz ligands coordinated to Mn2 and Mn2<sup>II</sup>. Structural omissions and color codes as in Figure 1. Symmetry codes: ii:  $-x+1, -y+1/2, z$ ; iii:  $-x+1, -y+1, -z$ .

are shown in the Supporting Information, Table S3. The distance between the Mn<sup>III</sup> ions (2.808(9)–2.823(1) Å) is the shortest intracluster Mn···Mn distance, all other exceed 3.14 Å. The angle between the outer Mn<sup>II</sup>–Mn<sup>II</sup> edges of the two Mn<sub>4</sub> tetrahedra in the {Mn<sup>II</sup><sub>4</sub>Mn<sup>III</sup><sub>2</sub>O<sub>2</sub>}<sup>10+</sup> core equals to 24.6, 25.7, and 26.1° for **1**, **2**, and **3**, respectively.

The geometrical parameters of cluster nuclei in **1–3** are virtually identical. All Mn centers are six-coordinated with near-octahedral geometry, with Mn–(μ<sub>4</sub>-O) bond lengths of 2.136(6)–2.192(5) Å (Mn<sup>II</sup>) and 1.880(5)–1.894(5) Å (Mn<sup>III</sup>). The four equatorial ligand positions of each terminal Mn<sup>II</sup> atoms are defined by three η<sup>1</sup>-O atoms of two μ<sub>2</sub>- and one μ<sub>3</sub>-carboxylate bridging ligands (2.084(9)–2.200(5) Å) and one by a η<sup>2</sup>-O atom of another μ<sub>3</sub>-bridge (2.240(3)–2.326(5) Å). The sixth vertex of each Mn<sup>II</sup> coordination octahedron is an oxygen or nitrogen atom of capping or spacer ligands. Each elongated Mn<sup>III</sup>O<sub>6</sub> octahedra are formed by the O atoms of bridging carboxylate ligands, namely, two η<sup>1</sup>-O atoms of two μ<sub>2</sub>-bridges (1.940(7)–1.974(5) Å), which together with μ<sub>4</sub>-O<sup>2-</sup> ions define the equatorial plane, and two η<sup>2</sup>-O atoms of the two μ<sub>3</sub>-carboxylate bridges (2.216(3)–2.274(5) Å) occupying axial positions. This Jahn–Teller elongation is expected for high-spin (d<sup>4</sup>) Mn<sup>III</sup> ions, with the axial Mn–O bonds exceeding the equatorial bonds by 0.242 Å.

Compound **1** crystallizes in monoclinic space group *C2/c*. The [Mn<sub>6</sub>O<sub>2</sub>(O<sub>2</sub>CCMe<sub>3</sub>)<sub>10</sub>] clusters reside in a general crystallographic position. Ethanol and pivalic acid molecules are capping the terminal *trans*-located Mn4 and Mn3 sites belonging to different Mn<sub>4</sub>O tetrahedra, Mn4–O26: 2.254(5) Å, Mn3–O20: 2.274(5) Å. The pivalic acid molecule is disordered over two positions in which it is stabilized by intramolecular hydrogen bonds (O21–H···O18: 2.604(1) Å and O21–H···O3: 2.703(2) Å). The na molecule serves as a exobidentate O,N-ligand and is coordinated via the amide oxygen atom and the pyridine nitrogen atom to the apical

(17) Brese, N. E.; O'Keefe, M. *Acta Crystallogr., Sect. B* **1991**, *B47*, 192.  
(18) Liu, W.; Thorp, H. H. *Inorg. Chem.* **1993**, *32*, 4102.

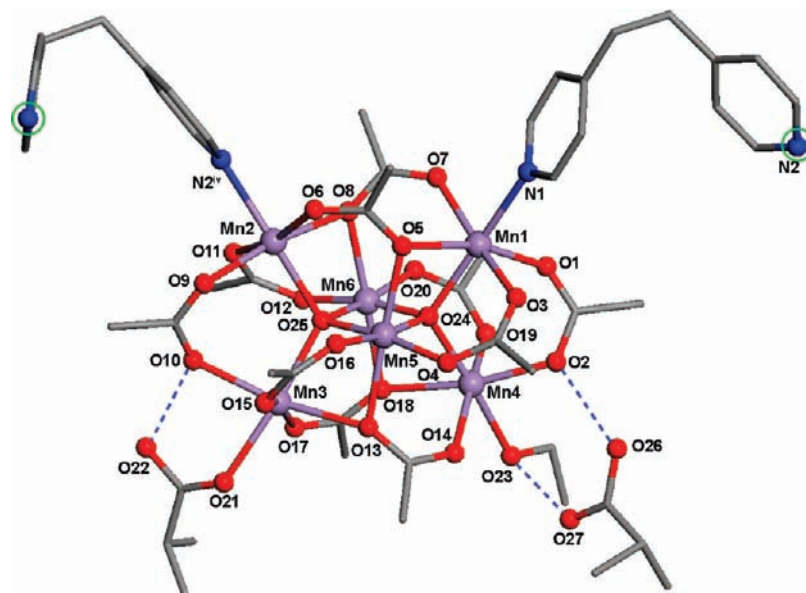


**Figure 3.** View of cluster in **3** with attached to Mn1 and Mn2 exobidentate bpe spacers, and H-bonded molecule of isobutyric acid. Structural omissions and color codes as in Figure 1. Symmetry code: *iv*:  $x-1/2, y, -z+3/2$ .

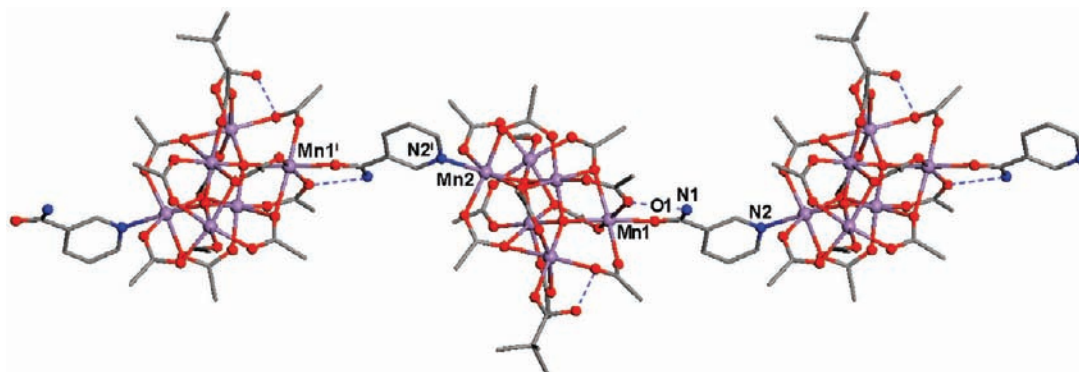


**Figure 4.** Polymeric chain in the structure of **1**. Mn1–O1: 2.209(5) Å, Mn2–N2': 2.323(6) Å. Structural omissions and color codes as in Figure 1. Symmetry code: *i*:  $-x+3/2, y-1/2, -z+1/2$ .

positions of Mn1 and Mn2 of neighboring cluster moieties, linking them to a polymeric chain along the crystallographic *b* axis, Figure 4. Repeating units in the chain are symmetry-related by 2-fold screw axis. The amide group of na is additionally bound to the cluster moiety by a N1–H···O4 (2.805(8) Å) hydrogen bond.

The intrachain intercluster Mn1<sup>i</sup>···Mn2 distance through the na spacer of 8.690(2) Å is the shortest intercluster Mn···Mn distance observed in the structure of **1**, but at least 0.6 Å longer than the Mn···Mn separation in a similar chain based on [Mn<sub>6</sub>O<sub>2</sub>Piv<sub>10</sub>]-cluster unit and nitroxide.<sup>12a</sup> The na molecules are attached to *trans*-positioned terminal Mn<sup>II</sup> atoms and oriented in head-to-tail fashion along the chain; hence, the chain has a preferential direction. The dihedral angle between pyridine and amide fragments of na equals to 27.8(5)°, indicating limited overlap between the carboxylate and the heteroaromatic  $\pi$  systems.

In the crystal of **1** the chains are packed as linear rods.<sup>19</sup> Parallel rods with identical direction of the na ligands form the sheets parallel to the *ab* crystallographic plane

(Figure 5). Sheets with alternating direction of na ligands stacked in ABAB fashion along the *c* crystallographic axis and create cavities filled by disordered ethanol and water solvent molecules. The total solvent-accessible volume for **1** was obtained using PLATON<sup>20</sup> by summing voxels that are more than 1.2 Å away from the framework and was estimated to be only 8.5%.

Compound **2** crystallizes in the tetragonal space group *I*<sub>4</sub>/*a*, with a crystallographic *C*<sub>2</sub> axis through O11 and O12  $\mu_4$ -O<sup>2-</sup> ions of the {Mn<sup>II</sup><sub>4</sub>Mn<sup>III</sup><sub>2</sub>O<sub>2</sub>}<sup>10+</sup> core; thus, only three Mn sites are symmetry-independent. Four outer Mn<sup>II</sup> ions are capped by pyrazine ligands. Two monodentate pyz ligands are attached to *cis*-situated Mn2 and Mn2<sup>ii</sup> within one Mn<sub>4</sub>O tetrahedron (Mn2–N2: 2.331(9) Å). Two other exobidentate pyz ligands reside each around the crystallographic center of symmetry and connect Mn1 and Mn1<sup>iii</sup> atoms of neighboring clusters to form a 1D zigzag chain (Mn1–N1: 2.297(8) Å), Figure 6.

The Mn<sub>4</sub>O tetrahedra with terminal (monodentate) and exobidentate bridging pyz ligands display different Mn<sup>II</sup>–( $\mu_4$ -O)–Mn<sup>II</sup> bond angles (Mn1–O11–Mn1<sup>ii</sup>: 114.9(3)°,

(19) Rosi, N. L.; Kim, J.; Eddaoudi, M.; Chen, B.; O'Keeffe, M.; Yaghi, O. M. *J. Am. Chem. Soc.* **2005**, *127*, 1504.

(20) Spek, A. L. *J. Appl. Crystallogr.* **2003**, *36*, 7.

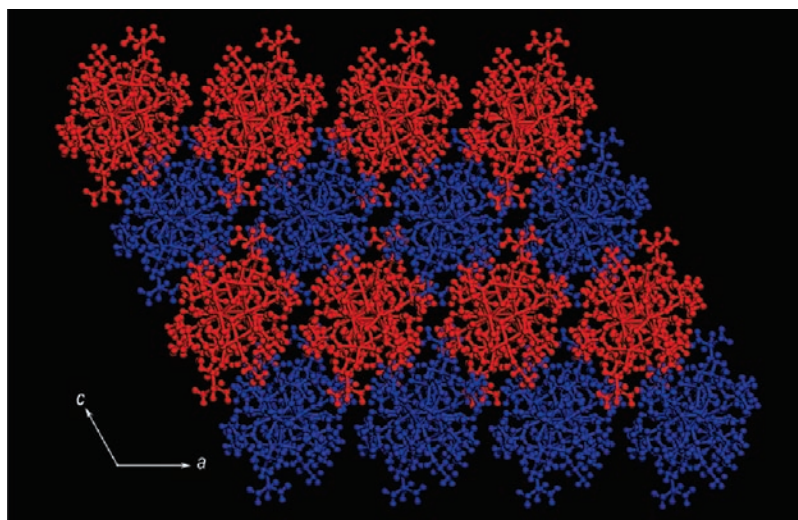


**Figure 5.** Ball-and-stick representation of packing diagram of **1** projected along *b*, that is, the polymer chain propagation axis. Red and blue colors indicate the antiparallel chains.

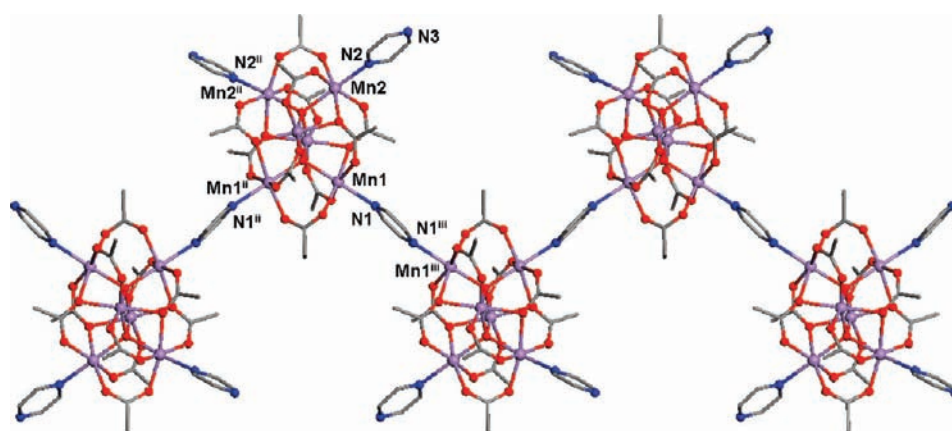


**Figure 6.** View of the 1D zigzag chain of **2** propagating along *b*. Methyl groups of bridging isobutyrate ligands, hydrogen atoms and solvate water molecules are omitted for clarity. Color codes as in Figure 1. Symmetry codes: *ii*:  $-x+1, -y+1/2, z$ ; *iii*:  $-x+1, -y+1, -z$ .

$\text{Mn2-O12-Mn2}^{\text{ii}}$ :  $118.1(4)^\circ$ ). The intercluster  $\text{Mn1}^{\text{iii}} \cdots \text{Mn1}^{\text{iii}}$  distance in the chain of  $7.288(3) \text{ \AA}$  is shorter than those in  $[\text{Mn}_6(\text{O})_2\text{Piv}_{10}]$ -based polymers incorporating nitroxide ( $8.069\text{--}8.119 \text{ \AA}$ )<sup>12</sup> or 4,4'-bipyridine ( $11.68 \text{ \AA}$ )<sup>13</sup> spacer ligands, but longer than that one of  $4.878(4) \text{ \AA}$  found in a zigzag chain constructed from related manganese oxide clusters bridged by propionato groups.<sup>14</sup> The shortest interchain  $\text{Mn} \cdots \text{Mn}$  distance in the structure of **2** is  $9.942(2) \text{ \AA}$ . In **2** chains run in perpendicular directions along the *a* and *b* crystallographic axes (Figure 7), and their packing creates closed cavities filled by disordered solvent water molecules.

Compound **3** crystallizes in the orthorhombic space group *Pbca*. The  $[\text{Mn}_6\text{O}_2(\text{O}_2\text{CCHMe}_2)_{10}]$  cluster nucleus resides in a general crystallographic position. The ethanol and isobutyric acid groups occupy the apical positions of outer *cis*-located Mn4 and Mn3 atoms (Mn4–O23:  $2.222(3) \text{ \AA}$ , Mn3–O21:  $2.271(3) \text{ \AA}$ ). The coordinated isobutyric acid additionally forms an O22–H $\cdots$ O10 ( $2.536(4) \text{ \AA}$ ) hydrogen bond with the cluster. In the solid state each cluster also associates with one solvent isobutyric acid molecule via O23–H $\cdots$ O27 ( $2.649(5) \text{ \AA}$ ) and O26–H $\cdots$ O2 ( $2.637(6) \text{ \AA}$ ) hydrogen bonds. The *exo*-bidentate bpe spacer ligand adopts a *gauche*-configuration with a torsion angle around the central C–C bond of  $66.4(6)^\circ$  and links neighboring glide plane-related

clusters in an unusual meander-like chain along the *a* axis (Figure 8). The chains are packed as parallel rods (Figure 9) in a manner similar to that found in the structure of **1**. Parallel rods with identical direction form the sheets parallel to the *ac* crystallographic plane. Such sheets with opposite direction of rods are stacked along the *b* crystallographic axis. Each cluster *cis*-coordinates two symmetry-related bpe molecules at apical positions of Mn1 and Mn2 (Mn1–N1:  $2.281(3) \text{ \AA}$ , Mn2–N2<sup>iv</sup>:  $2.273(3) \text{ \AA}$ ). The  $\text{Mn1}^{\text{iv}} \cdots \text{Mn2}$  distance through the bpe ligand equals to  $9.239(2) \text{ \AA}$ , while the shortest interchain  $\text{Mn} \cdots \text{Mn}$  distance is  $9.161(2) \text{ \AA}$ . The  $\text{Mn}-(\mu_4\text{-O})\text{-Mn}$  bond angles in the two  $\text{Mn}_4\text{O}$  tetrahedra of the cluster core are virtually identical (Supporting Information, Table S2).

**Magnetochemical Analysis.** Magnetic susceptibility data of the  $\{\text{Mn}_6\}$  cluster-based chains were evaluated based on the central assumption that intercluster magnetic exchange coupling, compared to intracluster exchange coupling, in compound **3** is negligible because of the absence of a conjugated  $\pi$  system extending to both N donor sites in the bpe ligand. Thus, coupling between adjacent  $\text{Mn}^{\text{II}}$  sites of neighboring  $\{\text{Mn}_6\}$  units is essentially limited to very weak dipole–dipole interactions, and the magnetic properties of **3** can be modeled with a simple isotropic Heisenberg exchange

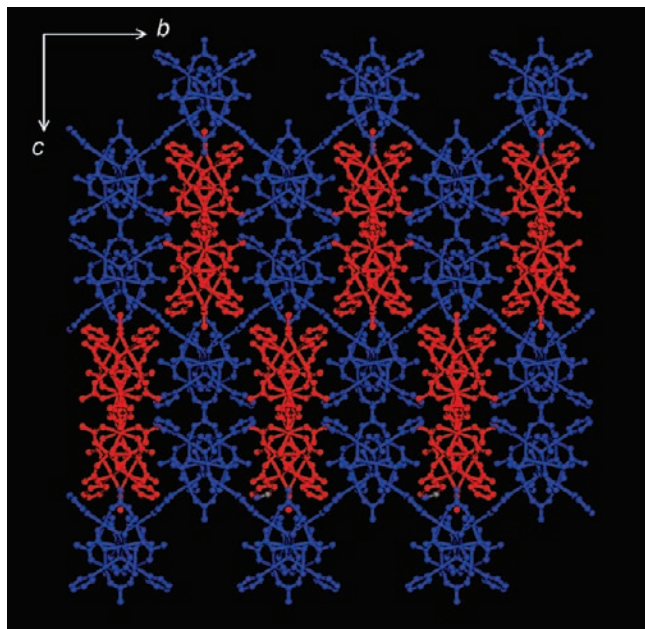


**Figure 7.** Ball-and-stick representation of packing diagram of **2** projected along the crystallographic *a* axis. Red and blue colors indicate the perpendicular propagation directions of the chains.

model. The  $\text{Mn}^{\text{III}}$  ions exhibit a  $^5\text{D}_0$  ground term with  $S = 2$  in octahedral high-spin complexes. The cubic ground state  $^5\text{E}$  implies Curie-type spin-only magnetism if the ligand field strength is weaker than  $Dq = 1500 \text{ cm}^{-1}$  and saturation effects play no significant role, resulting in a high-temperature limit of  $\chi T$  per  $\text{Mn}^{\text{III}}$  site of  $2.97 \text{ cm}^3 \text{ K mol}^{-1}$ . The octahedrally coordinated  $\text{Mn}^{\text{II}}$  ions ( $^6\text{A}_1$ ;  $^6\text{S}_{5/2}$  ground term) represent ideal spin-only  $S = 5/2$  centers ( $\chi_{\text{m}}T = 4.38 \text{ cm}^3 \text{ K mol}^{-1}$ ).

The general intracluster exchange coupling scheme for the  $\{\text{Mn}^{\text{III}}_2\text{Mn}^{\text{II}}_4\}$  spin clusters in compounds **1–3** (Figure 10) leads to the intracluster Heisenberg spin Hamiltonian

$$\begin{aligned}
 H_{\text{ex}} = & -2[J_1(S_1 \cdot S_2) \\
 & + J_2(S_1 \cdot S_3 + S_1 \cdot S_5 + S_2 \cdot S_4 + S_2 \cdot S_6) \\
 & + J_3(S_2 \cdot S_3 + S_2 \cdot S_5 + S_1 \cdot S_4 + S_1 \cdot S_6) \\
 & + J_4(S_3 \cdot S_4 + S_5 \cdot S_6)]
 \end{aligned}$$

that is limited to the dominant exchange pathways involving bridging oxo positions (Figure 10). Significantly weaker exchange, for example, between  $\text{Mn}2$  and  $\text{Mn}2'$  involving two carboxylate bridges in **1**, **2**, and **3**, is neglected. In addition, to avoid overparametrization of the model, the exchange constants for  $\text{Mn}^{\text{II}}-\text{Mn}^{\text{III}}$  exchange, mediated by a  $\mu_4$ -oxo center and a carboxylate group ( $J_3$ ) or mediated by a  $\mu_4$ -oxo center, a  $\mu_3$ -oxo center, and a carboxylate group ( $J_2$ ) are approximated to be identical.  $J_1$  quantifies the  $\text{Mn}^{\text{III}}-\text{Mn}^{\text{III}}$  exchange via two  $\mu_4$ -oxo centers,  $J_4$  the  $\text{Mn}^{\text{II}}-\text{Mn}^{\text{II}}$  exchange via one  $\mu_4$ -oxo center and a carboxylate linker.

Intercluster exchange interactions between the  $\{\text{Mn}^{\text{III}}_2\text{Mn}^{\text{II}}_4\}$  units are expected to be significant for compounds **1** and **2** incorporating linker groups with a conjugated  $\pi$  system (Table 1) and can be accounted for by a molecular field approximation,  $\chi_{\text{m}}^{-1} = \chi'_{\text{m}}^{-1}(B, C, \zeta, B_q^k, J_{\text{ex}}) - \lambda_{\text{mf}}$ ,

where  $\chi'_{\text{m}}$  represents the susceptibility contribution of the individual  $\{\text{Mn}_6\}$  units and  $\lambda_{\text{mf}}$  designates the molecular field parameter. Our computation framework CONDON was employed to model the temperature-dependent low-field susceptibility data for **1–3**.<sup>21</sup>

The temperature dependence of the low-field molar magnetic susceptibility  $\chi_{\text{m}}$  of **3** (Figure 11) exhibits a characteristic sharp maximum at 6.0 K, indicating dominant antiferromagnetic intracluster coupling. The  $\chi_{\text{m}}T$  value at 290 K of  $20.89 \text{ cm}^3 \text{ K mol}^{-1}$  is below the expected spin-only value of  $23.46 \text{ cm}^3 \text{ K mol}^{-1}$  for six isolated magnetic centers ( $4 \times \text{Mn}^{\text{II}}$  with  $S = 5/2$  and  $2 \times \text{Mn}^{\text{III}}$  with  $S = 2$ ;  $g = 2.0$ ). This is in agreement with room temperature  $\chi_{\text{m}}T$  values for other  $[\text{Mn}^{\text{III}}_2\text{Mn}^{\text{II}}_4\text{O}_2]^{10+}$  clusters with similar core structures.<sup>11g</sup>

The expected singlet ground state of **3** is confirmed by field-dependent magnetization measurements ( $B_0 = 0\text{--}5.0 \text{ T}$ ,  $2.0 \text{ K}$ ). Using CONDON, a least-squares fit to the experimental molar susceptibility data at 0.1 T for  $T = 2$  to 290 K yields all-antiferromagnetic exchange energies  $J_1 = -1.61 \text{ cm}^{-1}$ ,  $J_2 = J_3 = -0.89 \text{ cm}^{-1}$ , and  $J_4 = -1.23 \text{ cm}^{-1}$  (SQ = 0.5%), shown as red lines in Figure 11, and a singlet ground state follows from these calculations of the spin states, too. Note that, as expected, the addition of a molecular field approximation does not improve the fitting result.

The  $\chi_{\text{m}}T$  versus  $T$  plots for **1** and **2** (Figure 12) display room temperature values of 19.9 and  $17.8 \text{ cm}^3 \text{ K mol}^{-1}$ , respectively, primarily because of additional antiferromagnetic intercluster coupling ( $\lambda_{\text{MF}} < 0$ ). Note that for both compounds  $\chi_{\text{m}}$  reaches a maximum at 20 K (Figure 12, inset). As for **3**, the linear low-temperature field-dependence of the magnetization for these compounds suggests a singlet ground state. Approximating the intracluster interactions  $J_1\text{--}J_4$  for **1** and **2** as equal to **3**, the intermolecular exchange interactions between the  $[\text{Mn}^{\text{III}}_2\text{Mn}^{\text{II}}_4\text{O}_2]^{10+}$  units is then quantified by the molecular field approximation. The resulting least-squares fits yield  $\lambda_{\text{mf}}$  equal to  $-1.131 \text{ cm}^3 \text{ mol}^{-1}$  (**1**) and  $-1.508 \text{ cm}^3 \text{ mol}^{-1}$  (**2**). This 33% increase in antiferromagnetic exchange coupling is in line with both the decreasing  $\text{Mn} \cdots \text{Mn}$  distance of adjacent Mn sites in neighboring  $\{\text{Mn}_6\}$  clusters bridged by either nicotinamide (**1**: 8.69 Å) or pyrazine (**2**: 7.29 Å) and with the transition from bridging ligand with limited  $\pi$  overlap between the amide and the pyridyl groups to the fully planar aromatic  $\pi$  system in pyrazine.

## Conclusion

The reaction of  $[\text{Mn}^{\text{II}}_4\text{Mn}^{\text{III}}_2(\mu_4\text{-O})_2(\text{O}_2\text{CR})_{10}\text{L}_4]$  clusters with appropriate bridging ligands of different geometric flexibility results in the desired ligand metathesis reactions yielding coordination polymers. Surprisingly, despite the potential for cross-linking to 2D or 3D networks, the employed spacer ligands resulted exclusively in 1D polymer chains that are stacked in colinear or perpendicular propagation directions in the crystal lattices. While nicotinamide as bridging ligand produces nearly linear chains (**1**) and pyrazine produces zigzag chains (**2**), unusual *cis*-type coordination to 1,2-bis(4-pyridyl)ethane of the  $\{\text{Mn}_6\}$  clusters results in an unusual meander-type chain structure (**3**). Magnetochemical analysis of the reported three compounds on a spin-only level was based on the assumption of negligible intercluster interactions in **3** and

(21) Schilder, H.; Lueken, H. *J. Magn. Magn. Mater.* **2004**, *281*, 17.

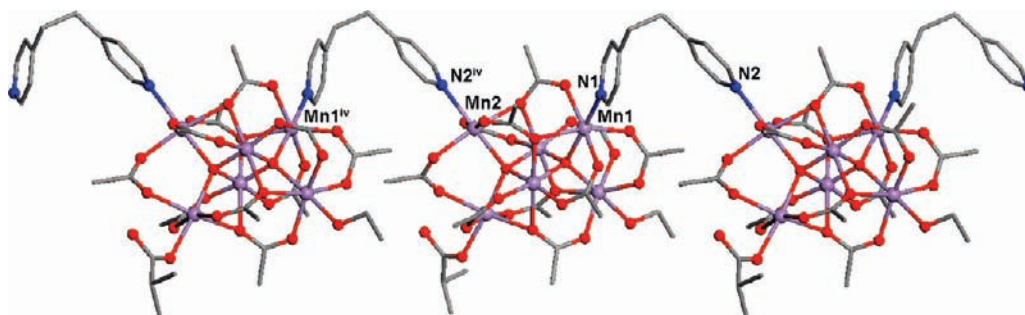


**Figure 8.** Meander-like chain in the structure of **3** is running along the *a* axis. Structural omissions and color codes as in Figure 1. Symmetry code: *iv*:  $x-1/2, y, -z+3/2$ .

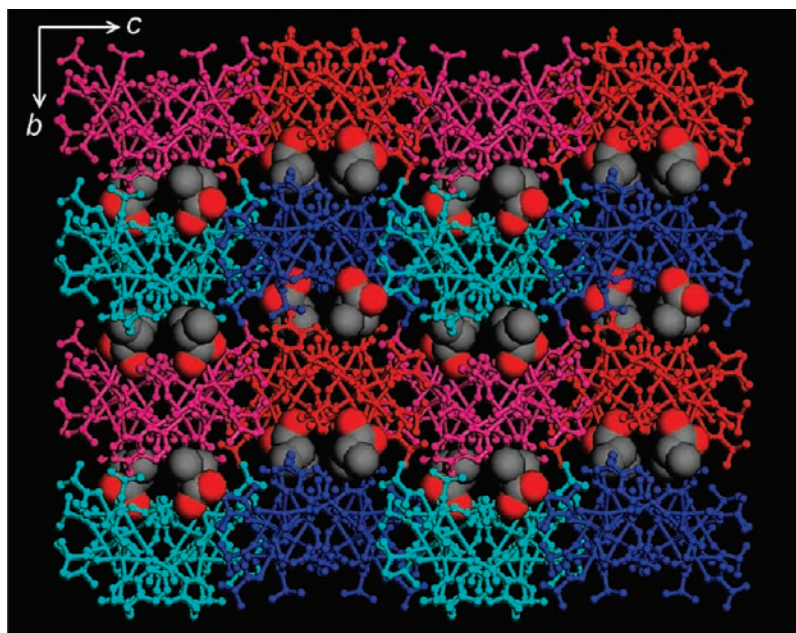


**Figure 9.** Ball-and-stick representation of packing diagram of **3** projected along the crystallographic *a* axis. Solvent isobutyric acid molecules are represented as space-filling models. Parallel chains are colored alternating pink and red or light blue and blue for improved clarity and visualization. Red and pink chains are antiparallel to blue and light blue chains. Hydrogen atoms omitted for clarity.

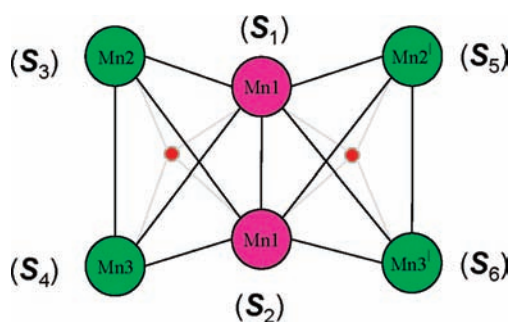


**Figure 10.** Intracuster magnetic coupling scheme for the  $\{Mn_6\}$  clusters in **1–3**. Only exchange pathways including one of the two  $\mu_4$ -oxo sites (small red circles) are indicated.

finds significant intercluster interactions in **1** and **2**, whereby the exchange strength correlates with the differences in the electronic  $\pi$  structure of pyrazine and nicotinamide.

### Experimental Section

**Materials and Methods.** All reactions were carried out under aerobic conditions using commercial grade solvents.  $[Mn(O_2CC-HMe_2)_2]^{15d}$  and  $[Mn(O_2CCMe_3)_2]^{15a}$  were synthesized as described

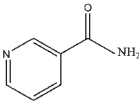
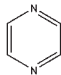

elsewhere. Commercially available ligands were used without further purification. Infrared spectra were recorded on a Perkin-Elmer Spectrum One spectrometer (KBr pellets,  $4000\text{--}400\text{ cm}^{-1}$ ). Thermogravimetric analysis and differential thermal analysis (TGA/DTA) measurements were carried out with a Mettler Toledo TGA/SDTA 851 in dry  $N_2$  ( $60\text{ mL min}^{-1}$ ; heating rate:  $10\text{ K min}^{-1}$ ). Magnetic susceptibility data were recorded using a Quantum Design MPMS-5XL SQUID magnetometer as a function of field (0.1 to 5.0 T) and temperature (2.0 to 290.0 K). Experimental data were corrected for sample holder (PTFE capsules) and diamagnetic contributions calculated from tabulated values ( $\chi_{\text{dia}}(\mathbf{1}) = -0.853 \times 10^{-3}\text{ cm}^3\text{ mol}^{-1}$ ;  $\chi_{\text{dia}}(\mathbf{2}) = -0.754 \times 10^{-3}\text{ cm}^3\text{ mol}^{-1}$ ;  $\chi_{\text{dia}}(\mathbf{3}) = -0.819 \times 10^{-3}\text{ cm}^3\text{ mol}^{-1}$ ).

**X-ray Crystallography.** For **1** data were collected on a Nonius Kappa CCD diffractometer whereas for **2** and **3** data were collected on a Bruker SMART CCD diffractometer, both employing graphite monochromatized Mo  $K\alpha$  radiation ( $\lambda = 0.71073\text{ \AA}$ ) and operating in  $\phi$  and  $\omega$  scan mode. Absorption correction was applied using SADABS.<sup>22</sup> Structures were solved by direct methods and refined on  $F^2$  using full-matrix least-squares.<sup>23</sup> Non-disordered non-H atoms were treated anisotropically in all structures.

(22) Sheldrick, G. M. *SADABS*; Bruker AXS Inc.: Madison, WI, 1997.

(23) (a) *SHELX86*; Sheldrick, G. M. *Acta Crystallogr., Sect. A* **1990**, *46*, 467. (b) Sheldrick, G. M. *SHELXL-97*; University of Göttingen: Göttingen, Germany, 1997; (c) Spek, A. L. *Acta Crystallogr., Sect. A* **1990**, *46*, C34.

Table 1. Magnetochemical Analysis Data

Complex	1	2	3
Inter-cluster linker group	nicotinamide 	pyrazine 	1,2-bis(4-pyridyl)ethane 
Inter-cluster distance / Å	8.690(2)	7.288(3)	9.239(2)
$\chi_{mf} / \text{cm}^3 \text{mol}^{-1}$	-1.131	-1.508	—
$SQ / \%$	1.6	2.3	0.5

$$SQ = \sqrt{\sum_{i=1}^n ([\chi_{obs}(i) - \chi_{cal}(i)] / \chi_{obs}(i))^2}$$

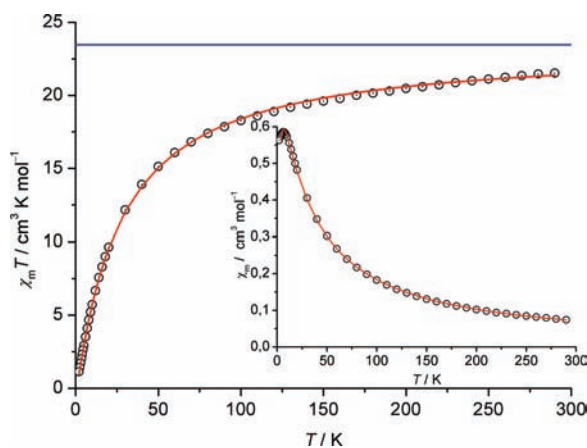


**Figure 11.** Temperature dependence of  $\chi_m T$  and molar susceptibility (inset) of **3** at an applied field of  $B_0 = 0.1$  T. Experimental data: circles, best fit to model Hamiltonian (see text): red line. The horizontal blue line represents the expected spin-only value for the six isolated magnetic centers per  $\{\text{Mn}_6\}$  cluster.

In **1**, methyl groups of four bridging pivalate ligands and pivalic acid molecule as well as solvent ethanol and water molecules were found to be disordered. The combined anisotropic/isotropic refinement has been used for non-H atoms in these disordered groups. Isotropic refinement was generally applied for the atoms with SOF of position less than 0.4, or when an anisotropic approach for partial site occupancy led to unstable refinement. Two bridging isobutyrate ligands in the asymmetrical part of the unit cell of **2** revealed disorders of isobutyl fragment of over two positions. Only for one of such disordered isobutyl fragment in minor occupancy position with SOF = 0.2 has the isotropic model of refinement been applied. Partial occupancy water molecules in four positions with SOF less than 0.2 in **2** have been refined isotropically. The disorder was also found for methyl groups of two bridging isobutyrate ligands in **3**. The hydrogen atoms in **1–3** were placed in calculated, ideal positions and refined as riding on their respective atoms. The hydrogen atom of hydroxyl group of disordered solvent ethanol molecule in **1** and hydrogen atoms of disordered water molecules in **1** and **2** have not been localized and included in the model of refinement. Unit-cell data and structure refinement details are listed in Table 2.

**Synthesis of Complexes.**  $\{[\text{Mn}_6\text{O}_2(\text{O}_2\text{CCMe}_3)_{10}(\text{Me}_3\text{CCO}_2\text{H})\cdot(\text{EtOH})(\text{na})\cdot\text{EtOH}\cdot\text{H}_2\text{O}]_n\}$  (**1**). To a solution of  $\text{Mn}(\text{O}_2\text{CCMe}_3)_2$  (0.16 g, 0.62 mmol) in 5 mL of MeCN, a solution of nicotinamide (0.16 g, 1.31 mmol) in 5 mL of EtOH was added. The resulting mixture was refluxed for 1 h. The crystals of **1** suitable for X-ray

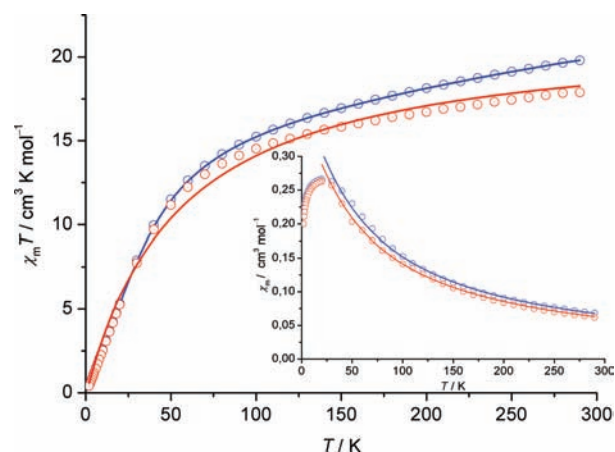


**Figure 12.** Temperature dependence of  $\chi_m T$  and molar susceptibility (inset) of **1** (blue) and **2** (red) at an applied field of  $B_0 = 0.1$  T. Experimental data: circles, best fits to model Hamiltonian; and molecular field approximation, solid lines.

Table 2. Crystallographic Data for Complexes 1–3

	1	2	3
formula	$\text{C}_{65}\text{H}_{120}\text{Mn}_6\text{N}_2\text{O}_{28}$	$\text{C}_{52}\text{H}_{86}\text{Mn}_6\text{N}_6\text{O}_{24}$	$\text{C}_{62}\text{H}_{104}\text{Mn}_6\text{N}_2\text{O}_{27}$
fw/g mol <sup>-1</sup>	1707.27	1508.91	1639.11
space group	<i>C2/c</i>	<i>I4<sub>1</sub>/a</i>	<i>Pbca</i>
<i>a</i> /Å	28.566(1)	18.782(3)	24.548(5)
<i>b</i> /Å	28.213(1)	18.782(3)	23.536(5)
<i>c</i> /Å	24.042(2)	41.025(10)	26.769(5)
$\beta$	119.329(3)°	90°	90°
<i>V</i> /Å <sup>3</sup>	16893(2)	14472(5)	15466(5)
<i>Z</i>	8	8	8
<i>T</i> /K	100	173	130
radiation/Å <sup>a</sup>	0.71073	0.71073	0.71073
$\rho_{\text{calcd}}/\text{g cm}^{-3}$	1.343	1.385	1.408
$\mu/\text{mm}^{-1}$	0.942	1.087	1.025
$R1^{b,c}$	0.0766	0.0696	0.0475
$wR2^d$	0.2379	0.2357	0.0973

<sup>a</sup> Graphite monochromator. <sup>b</sup>  $I > 2\sigma(I)$ . <sup>c</sup>  $R1 = \sum ||F_o| - |F_c|| / \sum |F_o|$ . <sup>d</sup>  $wR2 = [\sum w(F_o^2 - F_c^2)^2 / \sum w(F_o^2)^2]^{1/2}$ ,  $w = 1/[\sigma^2(F_o^2) + [(ap)^2 + bp]]$ , where  $p = [\max(F_o^2, O) + 2F_c^2]/3$ .

analysis were separated by filtration after 24 h, washed with MeCN, and dried in air (yield: 0.07 g, 41%). Elemental analysis, calculated (found) for  $\text{C}_{65}\text{H}_{120}\text{Mn}_6\text{N}_2\text{O}_{28}$ : C, 45.84 (45.73); H, 6.82 (7.08); N, 1.73 (1.64)%. IR (KBr, cm<sup>-1</sup>): 3499br.m, 2960s, 2927sh, 2871sh, 1682sh, 1591vs, 1483vs, 1421vs, 1374s, 1359s, 1227s, 1031w, 894w,



787w, 699w, 613s, 557w. UV/vis (powder reflection, Supporting Information, Figure S4):  $\lambda_{\text{max}} = 485 \text{ nm}$ .

$\{[\text{Mn}_6\text{O}_2(\text{O}_2\text{CCHMe}_2)_{10}(\text{pyz})_3 \cdot 2\text{H}_2\text{O}]_n\}$  (**2**). A mixture of  $\text{Mn}(\text{O}_2\text{CCHMe}_2)_2$  (0.11 g, 0.48 mmol), *N,N'*-bis(2-hydroxyethyl)ethylenediamine (0.07 g, 0.47 mmol) and pyrazine (0.08 g, 0.99 mmol) was refluxed in 10 mL of MeCN during 30 min. The resulting hot brown solution was filtered and left in a covered vial for several days. The formed brown crystals were filtered off, washed with MeCN, and dried in air (yield: 0.065 g, 54%). Elemental analysis, calculated (found) for  $\text{C}_{52}\text{H}_{86}\text{Mn}_6\text{N}_6\text{O}_{24}$ : C, 41.39 (41.07); H, 7.74 (7.35); N, 5.56 (5.39) %. IR data (KBr,  $\text{cm}^{-1}$ ): 3420br,m, 2969 m, 2929w, 2872w, 1585s, 1472 m, 1421s, 1372w, 1286 m, 1095w, 1044w, 938w, 611w, 544w.

$\{[\text{Mn}_6\text{O}_2(\text{O}_2\text{CCHMe}_2)_{10}(\text{Me}_2\text{CHCO}_2\text{H})(\text{EtOH})(\text{bpe}) \cdot \text{Me}_2\text{CHCO}_2\text{H}]_n\}$  (**3**). To a hot solution of  $\text{Mn}(\text{O}_2\text{CCHMe}_2)_2$  (0.11 g, 0.48 mmol) in 2.5 mL of EtOH was added a hot solution of 1.2-bis(4-pyridyl)ethane (0.045 g, 0.24 mmol) in 2.5 mL of THF. The resulting mixture was left in a covered vial for several days to give suitable for X-ray single crystals. The brown crystals of the title compounds were filtered off, washed with EtOH, and dried in air (yield: 0.09 g, 69%). Elemental analysis, calculated (found) for  $\text{C}_{62}\text{H}_{104}\text{Mn}_6\text{N}_2\text{O}_{27}$ : C, 45.43 (45.07); H, 6.39 (6.05); N, 1.70 (1.49)%. IR data (KBr,  $\text{cm}^{-1}$ ): 3425br,m, 2970 m, 2929sh, 2872sh, 1688sh, 1595vs, 1472s, 1421vs, 1371 m, 1284 m, 1255 m, 1169w, 1095 m, 1014w, 928w, 841w, 815w, 778w, 609 m, 546 m, 517w.

**Acknowledgment.** Funded by the Excellence Initiative of the German federal and state governments and supported by the Supreme Council for Science and Technological Development of R. Moldova (project 09.836.05.02A), the German Federal Ministry of Education and Research (project MDA 08/022), and the Academy of Sciences of Moldova (project No. 09.820.05.10GF). The authors thank Dr. Yu. Wang for the collection of crystallographic data sets for compound **3** and Dr. Michael Noyong for UV/Vis measurements.

**Supporting Information Available:** X-ray crystallographic data in CIF format for complexes **1–3**; IR and thermal analysis summaries, Mn···Mn distances (Table S1), selected bond lengths and angles (Table S2) details of BVS calculations (Table S3), ORTEP plots of asymmetric units (Figures S1–S3), the powder reflection UV/vis spectrum of **1** (Figure S4), and TGA/DTA graphs (Figures S5–S7). This material is available free of charge via the Internet at <http://pubs.acs.org>. Crystallographic data have been deposited with Cambridge Crystallographic Data Centre under nos. CCDC 744546–744548 for compounds **1–3**. Copies of this information may be obtained from CCDC, 12 Union Road, Cambridge, CB2 1EZ, U.K. (fax: +44–1233–336033; e-mail: [deposit@ccdc.cam.ac.uk](mailto:deposit@ccdc.cam.ac.uk) or [www: http://www.ccdc.cam.ac.uk](http://www.ccdc.cam.ac.uk)).